Polarization effects on the two-photon dissociation of HD^+ with two radiation fields in the presence of one and two intermediate resonant states

Banani Datta and S. S. Bhattacharyya
Atomic and Molecular Physics Section, Department of Materials Science, Indian Association for the Cultivation of Science, Calcutta 700032, India
(Received 1 December 1992)

The polarization dependence of resonant two-photon dissociation characteristics has been investigated for HD^+ excited from the ground state by two fields of different frequencies. The change in dissociation probability with field intensity and the dissociation line shape have been shown in the case of a single intermediate resonance for all possible combinations of polarizations. The photofragment energy spectra and the branching ratio between two possible continuum-energy states have been investigated for these polarization states when two intermediate resonances are present.

PACS number(s): 33.80.Wz, 33.60.−q, 33.10.−n

INTRODUCTION

During the past few years there has been a surge of interest in the theory of resonant transition to the continuum of a simple molecular system by single or multiphoton absorption in intense fields. In particular, photodissociation of the simplest one-electron molecular ion H_2^+ in intense fields have been extensively studied recently [1–9]. These authors have used both time-dependent [3] and time-independent nonperturbative approaches. The two approaches have been compared and their complementarity stressed [4]. In most of the time-independent approaches the dynamics of the dissociating molecule is determined by the behavior of the initial bound state in the field-dressed adiabatic electronic potentials obtained by diagonalization of the molecule-field Hamiltonian with various photon-number states. Only the lowest two molecular electronic states have been used in all such calculations.

In earlier works we have extensively studied resonant two-photon dissociation (TPD) of the isotopic variant HD^+ in single- [10] and two-frequency fields with one [11] and two [12] intermediate resonances. HD^+ qualitatively differs from H_2^+ in that it has a permanent dipole moment and hence a resonance with a bound vibrotational level of the $1s\sigma_g$ state is possible. Instead of working in the dressed adiabatic basis we used the resolvent operator formalism in which the dynamics of the bound resonant states were isolated by the use of a projection operator [13]. The dressed states in the projected basis were obtained by taking the effect of the states outside the basis set to the lowest nonvanishing order in both diagonal and off-diagonal matrix elements in this basis. This method somewhat restricted the upper limit of the intensities by neglecting the field-induced modifications of the states outside the basis set [11,12] as well as multiple transitions between states within and outside the basis set. However, this method allowed us to separate the effect of the two fields present by independently varying their intensities and frequencies, at the same time retaining the coherent character of the process. Also, unlike the other authors, we could include the effect of rotations on the intermediate and final states. These rotations play very important roles in determining the characteristics of a resonant process and in the present study we will be concerned with the polarization dependence of the process which is manifested through the change of symmetries of the rotational wave functions.

In a coherent resonant multiphoton excitation process the channels available in the continuum will depend upon successive values of the angular momentum quantum numbers of the resonant states as well as the polarizations of the lasers. For a given set of polarizations, the averaged excitation pattern can be obtained from a set of independent ladders having different dynamical behaviors in a field, one for each initial orientation of the atomic or molecular system [14]. In strong fields each of the excitation ladders is modified appreciably due to the different field-induced shifts and widths of the resonant states reached in that ladder for a particular initial orientation. These shifts and widths depend on the polarizations of the fields [15]. Also, repeated transitions between the states induced in any one ladder will result in further modification of the dynamical behavior of that ladder.

In our earlier works, mentioned above, we mainly studied dissociation line shapes and photofragment spectra for resonant TPD of HD^+ from a rotationless state. The two fields used had different intensities and frequencies but were parallelly plane polarized. In this paper we have used all possible combinations of polarizations of the two fields. Use of the same initial angular momentum state $J=0$ simplifies the calculation since the transition characteristics now depend on a single ladder only [14] and we show how different rotational wave functions of the intermediate resonance and final continuum states result in different TPD line shapes and photofragment spectra for different polarizations of the fields depending on their intensities. We demonstrate the variation of two-frequency resonant TPD probability and the photofragment spectra for selected values of radiation field intensi-

ties for one and two intermediate resonances, respectively.

In limiting cases the geometrical factors arising from the angular momentum quantum numbers and polarization indices in the transition cross section can be averaged out over several ladders and separated from the dynamical factors. Thus the angular momentum dependence of different branches of two-photon absorption lines in a rotating diatomic molecule were first studied for linearly and circularly polarized light by Bray and Hochstrasser [16] and Chen and Yeung [17]. For weak-field TPD through a resonant state also, the relative contributions of different final channels can be separated into dynamical and geometrical factors. The dynamical factors are determined from the radial parts of the dipole transition matrix elements on different potential-energy curves. The geometrical factors enter through the Clebsch-Gordan coefficients and reflect the orientation or alignment of a particular intermediate state and the difference in the total number of final channels available for a given set of polarizations. Chen and Yeung [18] and Banerjee *et al.* [19] have studied such polarization effects on weak-field resonance enhanced TPD for general values of J. However, for sufficiently strong fields no such straightforward separation of the total process into geometrical and dynamical factors will be possible. This is so because these geometrical and dynamical factors, in various matrix elements, enter the final equations being nonlinearly coupled. Thus the dynamical response as a whole is to be computed separately for each set of polarization for a given set of intensities where nonlinearities are appreciable.

In the following section we describe the different combinations of the fields and give a brief formulation of the problem. The results obtained for all these field combinations are presented in the last section.

FORMULATION

The detailed formulation for obtaining the transition probabilities and photofragment energy spectra in two-frequency resonant TPD have already been given for linear polarizations using the resolvent operator formalism [11,12]. Here we write only the three coupled equations for matrix elements of the resolvent operator G in the space defined by the initial and the resonant field-molecule states. For two photon transitions from an initial field-molecule state $|g,n_1,n_2\rangle$ to the dissociative continua $|c_i,n_1-1,n_2-1\rangle$ and $|c_i',n_1,n_2-2\rangle$ through the intermediate resonant states $|a_1,n_1-1,n_2\rangle$ and $|a_2,n_1,n_2-1\rangle$ these equations are

$$(x-\tilde{\delta}_0)G_{gg}-\tilde{\Omega}_1 G_{a_1 g}-\tilde{\Omega}_2 G_{a_2 g}=1 , \tag{1a}$$

$$-\tilde{\Omega}_1 G_{gg}+(x-\tilde{\delta}_1)G_{a_1 g}-\tilde{F}_{12}G_{a_2 g}=0 , \tag{1b}$$

$$-\tilde{\Omega}_2 G_{gg}-\tilde{F}_{21}G_{a_1 g}+(x-\tilde{\delta}_2)G_{a_2 g}=0 . \tag{1c}$$

Here $\tilde{\Omega}_j=\bar{D}_{ga_j}(1-i/q_j)$, $\tilde{\delta}_0=-(i/2)\gamma_g$, and $\tilde{\delta}_j=\delta_j-(i/2)\Gamma_{a_j}$ with $\delta_j=\bar{E}_{a_j}-\bar{E}_g$ where $\bar{E}_{a_j}=E_{a_j}+F_{a_j}$, $\bar{E}_g=E_g+f_g$, and $j=1,2$. The quantities γ_g,Γ_{a_i} are the widths and f_g and F_{a_i} are the shifts of the initial and resonant states, respectively, due to the presence of two fields. $\bar{F}_{12}$ ($\bar{F}_{21}$) is the complex two-photon Raman-like coupling between two resonant states and q_j is the Fano asymmetry parameter for the resonant state a_j defined in the usual way. The shifts and widths have been calculated, as usual, in the lowest nonvanishing order of the interaction Hamiltonian with the rotating-wave approximation [11,12].

The three equations [Eq. (1)] will be reduced into two equations if one of the two lasers is highly detuned. In general the roots of the secular equation corresponding to Eq. (1) will define three complex dressed energy eigenvalues whose positions and widths govern the dissociation characteristics.

To calculate the radiation field induced quantities in Eq. (1) we have used the general expression of the interaction operator for linearly and circularly polarized radiation fields [20]

$$\hat{\epsilon}\cdot\mathbf{d}=\sum_{\lambda=-1}^{1} d_\lambda D_{p\lambda}^{1*}(\phi_r,\theta_r,0)(1-2\delta_{p1}) , \tag{2}$$

where the polarization index $p=0$ for parallel linear and $p=\pm 1$ for two senses of circular polarization. A linear polarization perpendicular to the Z axis can be written as a linear combination of the expressions for two circular polarizations. We denote the polarization indices of the two fields of intensities I_1 of frequency ω_1 and I_2 of frequency ω_2 by p_1 and p_2, respectively. In our calculations the molecular state $v_g=0,J_g=0$ of the $1s\sigma_g$ electronic state has been taken as the initial state $|g\rangle$ while $|a_1\rangle$ and $|a_2\rangle$ respectively denote the states $v=6,J=1$ and $v=14,J=1$. Either both the fields of frequencies ω_1 and ω_2 are in near resonance with $|a_1\rangle$ and $|a_2\rangle$, respectively, or only the field ω_2 is in resonance with $|a_2\rangle$. The six combinations of polarizations (p_1 and p_2) used are as follows.

(i) Both the fields are linearly polarized parallel to space-fixed Z axis. For this case, only $\Delta M=0$ transitions are involved, where M is the projection of angular momentum J on the space-fixed Z axis. So the polarization indices are $p_1=0$ and $p_2=0$.

(ii) When the fields are perpendicularly polarized, the polarization direction of the field of ω_2 frequency is taken along space-fixed Z axis. Then both the magnetic sublevels $|J_1=1,M_1=1\rangle$ and $|J_1=1,M_1=-1\rangle$ of the resonant $|a_1,n_1-1,n_2\rangle$ state are coherently excited by the ω_1 frequency field. Two states $|+\rangle$ and $|-\rangle$ are formed by linear combinations of $|J_1=1,M_1=1\rangle$ and $|J_1=1,M_1=-1\rangle$ sublevels of $|a_1\rangle$:

$$|+\rangle=\frac{1}{\sqrt{2}}[|a_1,n_1-1,n_2,J_1=1,M_1=1\rangle + |a_1,n_1-1,n_2,J_1=1,M_1=-1\rangle] \tag{3a}$$

and

$$|-\rangle=\frac{1}{\sqrt{2}}[|a_1,n_1-1,n_2,J_1=1,M_1=1\rangle - |a_1,n_1-1,n_2,J_1=1,M_1=-1\rangle] . \tag{3b}$$

Only the $|-\rangle$ state is coupled with the initial state $|g,n_1,n_2,J=0,M=0\rangle$ and the two-photon coupling between $|+\rangle$ and $|-\rangle$ states is forbidden. The polarization indices for this case are $p_1=+1$ and $p_1=-1$ acting together, and $p_2=0$.

(iii) When both the fields are circularly polarized in the same sense and the directions of propagation of both are parallel to the space-fixed Z axis, the polarization vector lies on the XY plane. For this case only $\Delta M=1$ (or -1) will be involved and we can take $p_1=1$ and $p_2=1$.

(iv) This is the same as the combination (3), but the sense of polarizations of the two circularly polarized waves are opposite. Then $p_1=1$ and $p_2=-1$.

(v) The field of frequency ω_1 is linearly polarized along the space-fixed Z axis and the circularly polarized field of frequency ω_2 is propagating parallel to Z axis. For this arrangement we shall have $p_1=0$ and $p_2=1$.

(vi) This is the same as the combination (5), but now the ω_1 frequency field is circularly polarized and the ω_2 frequency field is linearly polarized along space fixed Z axis. Hence $p_1=1$ and $p_2=0$.

Using the corresponding values of p_1 and p_2 for the six polarization sets we have to obtain the expressions of the field-induced quantities appearing in Eq. (1) and parameterizing the dynamics of TPD. The radial parts of the matrix elements involved are independent of radiation field polarizations. However, the integration over the angular coordinates will give different results for different combinations of polarizations since the relevant magnetic quantum numbers of the resonant state and the final state will be different in each case. Using Eq. (2) and the bound- and free-state molecular wave functions [21] the expressions for bound-bound, bound-free, and ground-to-continuum two-photon matrix elements have been obtained for the specialized case of $J_g=0,M_g=0$ only. The expressions of the different field-induced parameters evaluated from these matrix elements by integration over all directions of motion in the continuum are expressed in the following form:

$$D_{a_k g}=\left[\frac{2\pi I_k}{c}\right]^{1/2} A_{ag} R_{a_k g} \ , \tag{4a}$$

$$\Gamma_{a_k}=2\pi(2\pi I_s/c)\,A_{\Gamma_a}\sum_i |R_{a_k c_i}|^2_{E=E_{A_k}+\omega_s} + \delta_{k2}2\pi(2\pi I_2/c)\,A'_{\Gamma_a}\sum_i |R_{a_k c_i'}|^2_{E=E_{A_k}+\omega_2} \ , \tag{4b}$$

$$F_{a_k}=(2\pi I_s/c)\,A_{F_a}\sum_i P\int |R_{a_k c_i}|^2 dE_{C_i}/(E_{A_k}+\omega_s-E_{C_i}) + (2\pi I_2/c)\,A'_{F_a} \times\sum_i P\int |R_{a_k c_i'}|^2 dE_{C_i'}/(E_{A_k}+\omega_2-E_{C_i'}) \ . \tag{4c}$$

Here $s=2$ for $k=1$ and $s=1$ for $k=2$. The molecular state energies of the resonant and final states now have been denoted by E_{A_k} and E_{C_i},

$$\gamma_g=2\pi(2\pi I_1/c)(2\pi I_2/c)\,A_{\gamma_g}\sum_i |R^{(2)}_{c_i g}|^2 + 2\pi(2\pi I_2/c)^2 A'_{\gamma_g}\sum_i |R^{(2)}_{c_i' g}|^2 \ , \tag{4d}$$

$$f_g=(2\pi I_1/c)\,A_{f_g}\sum_{b_1}|R_{g b_1}|^2 + (2\pi I_2/c)\,A'_{f_g}\sum_{b_2}|R_{g b_2}|^2 \ , \tag{4e}$$

$$q_{kII}=\frac{c}{\pi(2\pi I_2)}A_{q_I}\frac{R_{a_k g}}{R_{a_k c_i}R^{(2)}_{c_i g}} \ , \tag{4f}$$

$$q_{kII}=\delta_{k2}\frac{c}{\pi\sqrt{(2\pi I_1)}\sqrt{(2\pi I_2)}}A_{q_{II}}\frac{R_{a_k g}}{R_{a_k c_i'}R^{(2)}_{c_i' g}} \ , \tag{4g}$$

and

$$\frac{1}{q_k}=\frac{1}{q_{kI}}+\frac{1}{q_{kII}} \ , \tag{4h}$$

where the intensity $I=(c/2\pi)F^2$. F is the half-amplitude of the radiation field.

Here the parameters are expressed in terms of intensity factors, geometrical factors (A's), and functions of purely radial matrix elements which are denoted by the R's. All the radial matrix elements have been evaluated in the velocity gauge, as usual. $R^{(2)}_{c_i g}$, etc. are the radial two-photon matrix elements from $|g\rangle$ to $|c_i\rangle$. $|b_1\rangle$ and $|b_2\rangle$ define a complete set of nonresonant states dipole connected to $|g\rangle$ by absorption of a single photon of frequency ω_1 and ω_2, respectively. The index i in $|c_i\rangle$ and $|c_i'\rangle$ differentiates the continuum states of nuclear motion on $1s\sigma_g$ and $2p\sigma_u$ potential surfaces of HD^+. The geometrical factors (A's), arising from the Clebsch-Gordan coefficients have been tabulated in Table I for all polarization combinations for the initial state $J=0$ as before. Both the intermediate resonant states have $J=1$. For HD^+ only $\Sigma\rightarrow\Sigma\rightarrow\Sigma$ transitions are involved and hence all Λ values are zero. For each polarization combination the roots of the secular equation are determined. The transition probabilities and the photofragment energy spectra are then obtained in the usual way.

RESULTS AND DISCUSSIONS

Using Table I for different polarization sets, we have studied (a) the intensity dependence and line shape of TPD when the $(v=14,J=1)$ level is resonantly coupled with the $(v=0,J=0)$ level and (b) TPD photofragment energy spectra when two resonant states $(v=6,J=1)$ and $(v=14,J=1)$ are resonantly coupled with the $(v=0,J=0)$ state.

Let us consider case (a) first. The resonant state $(v=14,J=1)$ is coupled with the $(v=0,J=0)$ state by F_2 field of polarization index p_2 and frequency ω_2. Figure 1 shows the dissociation probabilities as functions of the half-amplitude F_1 of the field of frequency ω_1 for $F_2=10^{-3}$ a.u. at the same real time of 10 ns and for $\delta=0$.

TABLE I. The molecular parameters using different polarizations p_1 and p_2 of two radiation fields for the intermediate resonant states ($v=14, J=1$) and ($v=6, J=1$).

Set no.	1	2	3	4	5	6
Polarization sets	$p_1=0$ $p_2=0$	$p_1=\pm1$ $p_2=0$	$p_1=1$ $p_2=1$	$p_1=1$ $p_2=-1$	$p_1=0$ $p_2=1$	$p_1=1$ $p_2=0$
			Parameters for ($v=14, J=1$) level			
A_{ag}	$-1/\sqrt{3}$	$-1/\sqrt{3}$	$1/\sqrt{3}$	$-1/\sqrt{3}$	$1/\sqrt{3}$	$-1/\sqrt{3}$
A_{r_a}	3 /5	2/5	2/5	2/5	1/15	1/15
A'_{r_a}	3/5	3/5	2/5	2/5	2/15	1/5
A_{F_a}	3/5	2/5	2/5	2/5	1/15	1/15
A'_{F_a}	3/5	3/5	2/5	2/5	2/15	1/5
$A_{q_{\mathrm{I}}}$	5/3	$-5/4$	$-5/2$	$-5/4$	5/2	$-5\sqrt{2}/4$
$A_{q_{\mathrm{II}}}$	5/3	5/3	$-5/2$	$-5/2$	$-5/2$	5/3
			Parameters for ($v=6, J=1$) level			
A_{ag}	$-1/\sqrt{3}$	$\sqrt{2/3}$	$1/\sqrt{3}$	$1/\sqrt{3}$	$-1/\sqrt{3}$	$1/\sqrt{3}$
A_{r_a}	3/5	1/5	2/5	2/5	1/5	1/5
A_{F_a}	3/5	8/45	2/5	2/5	3/5	2/5
A'_{F_a}	3/5	1/5	2/5	2/5	1/5	1/5
A_q	5/3	∞	$-5/2$	$-15/2$	$-5/(2\sqrt{2})$	5/2
A_{γ_g}	1/5	2/15	2/15	2/15	4/15	4/15
A'_{γ_g}	1/5	1/5	2/15	2/15	2/15	1/5
A_{f_g}	1/3	2/3	1/3	1/3	1/3	1/3
A'_{f_g}	1/3	1/3	1/3	1/3	1/3	1/3
$A_{F_{12}}$	3/5	$\sqrt{2}/5$	$-2/5$	1/15	$-1/5$	$\sqrt{2}/5$

It may be mentioned that $F=10^{-3}$ a.u. corresponds to an intensity of about 3×10^{12} W/cm^2. Since the shifts are different for different sets of polarization, for keeping $\delta=0$ the frequency of the radiation field has to be changed. Since the set of equations (1) involves only the detuning δ from the shifted energy values, the final results will be functions of δ only. Hence the results for different sets should be compared for the same values of the detuning δ to assess the role of the changes in transition strengths and couplings.

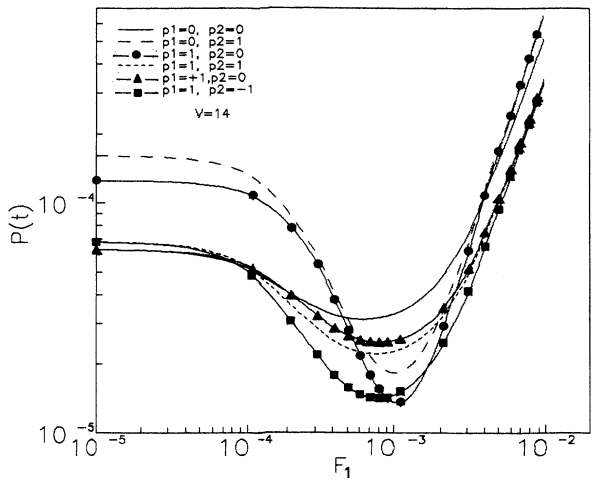

FIG. 1. Dissociation probability $P(t)$ against the half-amplitude F_1 of the nonresonant field (in a.u.) for resonance with $v=14$ at $\delta=0$, and $t=10$ ns for the six polarization sets. The intensity I is proportional to F^2. F_2 is fixed at 10^{-3} a.u. and corresponds to an intensity of very nearly 3×10^{12} W/cm^2.

In the lower F_1 region transition probabilities for the sets (5) ($p_1=0, p_2=1$) and (6) ($p_1=1, p_2=0$) are larger than that using two linearly polarized fields ($p_1=0, p_2=0$). On the other hand, the probability from sets (2)–(4) are nearly equal in magnitude in this region. For this resonant state the resonant coupling D_{ga} is much smaller than the width Γ_a of the resonant state and thus the roots of the secular equation will be obtained from the expansions [11]

$$x_1=\frac{2D_{ga}^2}{\Gamma_a(1+y^2)}\left[\frac{2}{q}+y\left[1-\frac{1}{q^2}\right]\right] -i\left[\frac{\gamma_g}{2}+\frac{2D_{ga}^2}{\Gamma_a(1+y^2)}\left[1-\frac{2y}{q}-\frac{1}{q^2}\right]\right], \quad (5a)$$

$$x_2=\frac{y\Gamma_a}{2}-\frac{2D_{ga}^2}{\Gamma_a(1+y^2)}\left[\frac{2}{q}+y\left[1-\frac{1}{q^2}\right]\right] -i\left[\frac{\Gamma_a}{2}-\frac{2D_{ga}^2}{\Gamma_a(1+y^2)}\left[1-\frac{2y}{q}-\frac{1}{q^2}\right]\right], \quad (5b)$$

where $y=\delta/(\Gamma_a/2)$.

For low values of F_1, γ_g and D_{ag}^2/Γ_a are roughly comparable to each other and since γ_g and Γ_a are mainly determined from F_2, the dissociation probability is in-

dependent of F_1. The relative magnitudes of $P(t)$ for different (p_1,p_2) combinations depend on the geometrical coefficients related to γ_g and Γ_a. Since geometrical coefficients in Γ_a are smaller for the sets (5) and (6) compared to others, the probability for these sets are larger in magnitude. At larger F_1 the contribution from F_1 to Γ_a and γ_g becomes appreciable and $P(t)$ decreases with an increase of F_1. Since the geometrical coefficients are different in two energy channels c_i and c_i', the rates of decrease of $P(t)$ are not the same for different sets. The probability curves for all the polarization sets show minima near $F=10^{-3}$ a.u. The curves for sets (5) and (6) cross the other curves and for intermediate values of the nonresonant field, the dissociation probabilities for one linear and one circularly polarized field can be lower than those obtained for other combinations. As discussed in [11] the transition probabilities increase with increase in the intensity of the F_1 field for $F_1 > 2\times 10^{-3}$ a.u., where nonresonant two-photon transitions start playing the more important part in determining dissociation probabilities. This can be explained by noting that for very large values of F_1, γ_g (increasing with F_1) becomes larger than D_{ag}^2/Γ_a (which decreases with F_1), causing an increase in the magnitude of the imaginary part of x_1 in Eq. (5a), which in turn causes increase of $P(t)$'s with the field. Geometrical coefficients of γ_g are larger for the sets (5) and (6), and a linearly and a circularly polarized radiation at right angles again give larger dissociation compared to others for high intensities of the nonresonant field.

In Figs. 2 and 3 the dissociation rates are plotted against normalized detuning (in units of $\Gamma_a/2$) for the six polarization sets. Because of the difference in the shifts and widths the real frequency range of the incident radiation will be different for different sets of polarizations with the same relative detuning range. Figure 2 shows

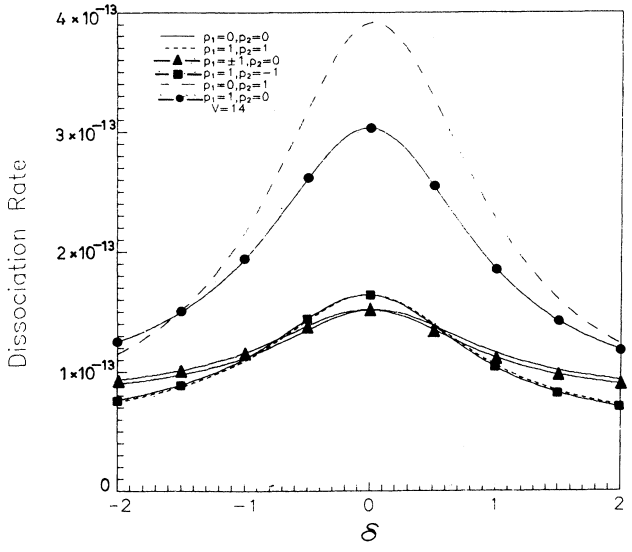

FIG. 2. Dissociation rate against δ (in units of $\Gamma_a/2$) with $v=14$ and $F_1=10^{-5}$ and $F_2=10^{-3}$ a.u.

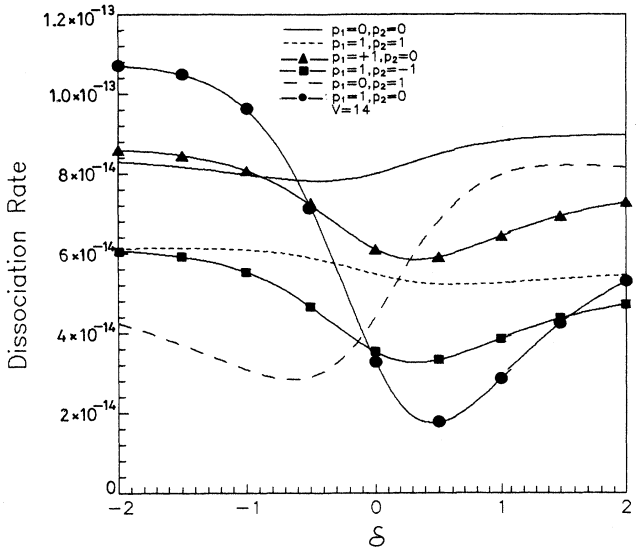

FIG. 3. Same as Fig. 2, except for $F_1=10^{-3}$ and $F_2=10^{-3}$ a.u.

the transition rate for $F_1=10^{-5}$ and $F_2=10^{-3}$ a.u. For these values of fields γ_g is comparable to D_{ag}^2/Γ_a and q is large. Due to the large value of q the curves are almost symmetrical around $\delta=0$. Small asymmetry arises at larger $|\delta|$ due to the effect of the second term in the imaginary part of Eq. (5a). The value of Γ_a for each case can be calculated by combining Table I of [11] with Table I of the present paper. For this particular combination of intensities the maximum width of the resonant state obtained is 0.38 cm^{-1} for parallel polarizations. The minimum width is 0.084 cm^{-1} for linear and circular polarizations of F_1 and F_2, respectively. Thus, though the dissociation line shapes are similar for different sets, both the peak value and the linewidth of the dissociation rate differ from set to set. The narrowest line is obtained by using circular and linear polarizations for the resonant and nonresonant fields, respectively.

In Fig. 3 the dissociative transition line shapes have been shown for $F_1=10^{-3}$ and $F_2=10^{-3}$ a.u. All the curves are asymmetric functions of δ. Maximum asymmetry is shown by the curves from sets (5) and (6). For these values of F_1 and F_2 all the parameters strongly depend on both F_1 and F_2. As q is very small, the second and third terms of the imaginary parts of Eq. (5a), which cause the asymmetry, are dominant. The maximum and minimum values of the width of the resonant state now are 31.6 cm^{-1} (for parallel polarizations of the two fields) and 3.6 cm^{-1} (for F_1 linearly and F_2 circularly polarized). In this case not only the widths but also the dissociation line shapes will be very different for the different sets of polarizations. All the lines will be broad, but it is not possible to indicate their widths from Fig. 3, since for larger values of the detuning the projection operator defining the resonant basis will have to be modified.

The photofragments produced using single frequency lasers will not all have the same kinetic energies but in-

stead will show a finite spread. A similar spread in photoelectron spectra with single-frequency lasers for different configurations and couplings between the resonant bound states and the continuum for model ionizing and autoionizing like situations has already been investigated by various authors [22–24]. We start with an initial ground-state wave function with a well-defined energy in the absence of external fields. Switching on the interactions will project this wave function on the laser dressed states, which are themselves mixtures of various field-molecule states included in our basis and variously broadened by what can be termed as laser-induced predissociationlike interactions. The evolution of the projections to various continuum wave functions then define the kinetic-energy spectrum [5]. Nice examples of photofragment energy distribution for multiphoton dissociation of H_2^+ occurring due to the projection of the initial field-free wave packet on the eigenstates of laser-dressed adiabatic potentials are given by Mies *et al.* [4–6]. In the limit of full dissociation, i.e., at $t \rightarrow \infty$, uncertainties in the molecular-energy component of the dressed states will be reflected in the long-time photofragment energy spectrum. For substantially shorter times the rapidly dissociated component will be distributed over a broader energy range.

When both lasers resonantly coupled different excited states (themselves coupled by complex Raman-like couplings) the dressed-state structure will be more interesting. Accordingly we consider the photofragment energy spectra for case (b) where both the states ($v=6, J=1$) and ($v=14, J=1$) are resonantly coupled with the initial state ($v=0, J=0$) by the fields F_1 and F_2, respectively. Figure 4 shows the long-time spectrum $W(\varepsilon)$, plotted against ε ($=E_C-E_G-\omega_1-\omega_2$) for $F_1=10^{-3}$ and $F_2=10^{-4}$ a.u. and at $\delta_1=\delta_2=0$ in the lower-energy channel c of the

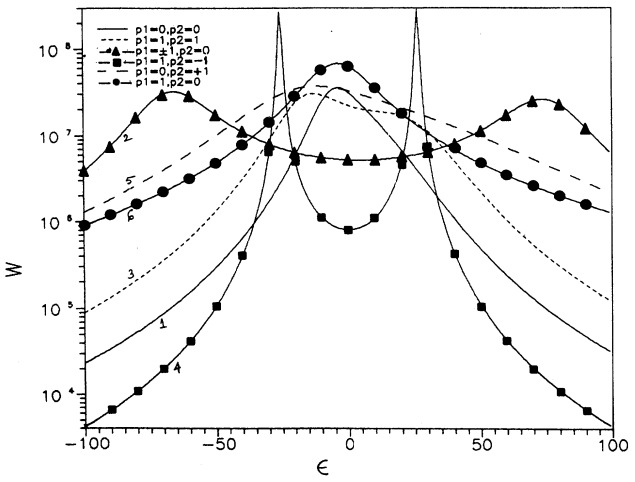

FIG. 4. Long-time energy distribution W of the photofragments against ε (in units of Γ_{a_1}) for simultaneous resonance with $v=6$ and $v=14$ for six polarization combinations and $F_1=10^{-3}$ and $F_2=10^{-4}$ a.u. at $\delta_1=0$ and $\delta_2=0$. The final electronic state is $2p\sigma_u$.

electronic state $2p\sigma_u$. The difference ε between the continuum energy and the undressed ground state plus photon energies is measured in units of linewidth Γ_a, which is here different for different combinations. The energy spectra for the higher-energy channel [$W'(\varepsilon')$] is similar, but their magnitudes are lower by 3 to 4 orders.

The total-energy range in Fig. (4) varies from a maximum of about 5.93×10^{-6} eV for parallel polarizations to a minimum of about 6.6×10^{-7} eV for a linear and a circular polarization. The final photofragment energy is around 0.9 eV. By staying within the framework of the Born-Oppenheimer approximation we are compelled to neglect the nonadiabatic couplings between the $1s\sigma_g$ and $2p\sigma_u$ states removing the degeneracy between the two asymptotic energies in the $H^+ + D$ and $D^+ + H$ channels. However, the resonant states will be affected little by this nonadiabatic coupling [25] and since the final energy is well above the threshold and since two-photon transitions play major roles only above the intensities considered here we do not consider the distribution of the photofragments between these two asymptotic states.

In [12] we obtained both unimodal and bimodal structures of the spectrum by varying the intensities of two parallel linearly polarized fields. The positions of the peaks approximately correspond to the energies of the dressed states and the peak heights change inversely with the width of those states. Here, by changing the polarizations keeping the field intensities and the detunings same, completely different shapes are obtained. For the polarization sets 1 ($p_1=0, p_2=0$), 5 ($p_1=0, p_2=1$), and 6 ($p_1=1, p_2=0$) we get spectra with a single peak. For the first two sets the position and width of two dressed states are almost equal. The single-peaked spectra arise due to the superposition of two peaks whose widths are larger than their separation. The third root has a very large imaginary part and does not contribute any peak. Because of the smallness of Γ_{a_1} and the consequent contraction of the scale, the spectrum for set 5 ($p_1=0, p_2=1$) looks much more diffused. However, for the set 6 ($p_1=1, p_2=0$), Γ_1 is the same as for $p_1=0, p_2=\pm1$ but only the root at $\varepsilon=-4$ contributes a peak. The two other peaks should be smaller by several orders of magnitude due to the large imaginary part of the corresponding roots and cannot be seen. The set 3 ($p_1=1, p_2=1$) exhibits a structure in which the existence of the two peaks is just discernible because of the comparability of their widths and separations. Once again, the third root will not contribute anything due to its large imaginary part. Since Γ_{a_1} here is six times the value of Γ_{a_1} for the two sets 5 and 6, the absolute separation between the roots is much larger.

The two bimodal structures in the spectra arise for the sets 2 ($p_1=\pm1, p_2=0$) and 4 ($p_1=1, p_2=-1$). The values of Γ_{a_1} for these sets are equal to that for the set 3 ($p_1=1, p_2=1$). In both cases we get two well-separated roots approximately symmetrically located on both sides of $\varepsilon=0$ with nearly the same magnitude of the imaginary parts. This results in two peaks. The third root always has a very large imaginary part and no peak in the spectrum appears corresponding to the position (real part) of

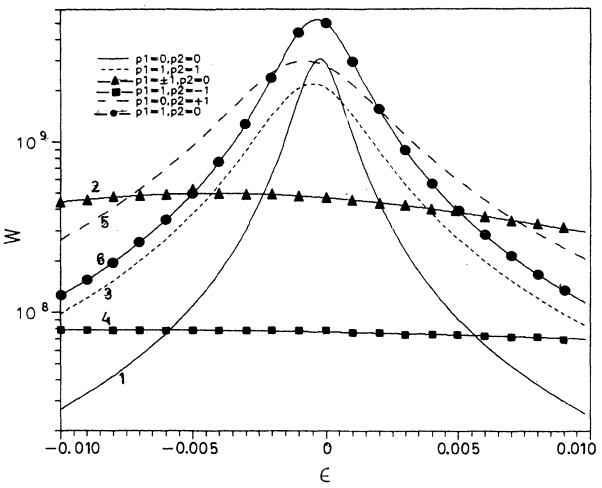

FIG. 5. Same as Fig. 4, except for $F_1=10^{-3}$ and $F_2=10^{-3}$ a.u.

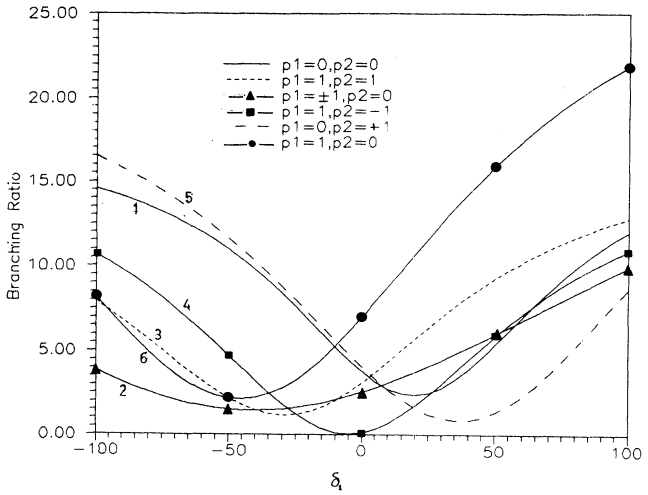

FIG. 6. Branching ratio plotted against δ_1 for $F_1=5\times10^{-5}$ and $F_2=10^{-3}$ a.u. at $\delta_2=0$.

this root.

The energy distributions obtained for $F_1=10^{-3}$ and $F_2=10^{-3}$ a.u. are shown in Fig. 5. For these strong fields the shift and width of one of the dressed states is much smaller compared to other two and a single peak near $\varepsilon=0$ results for all polarization sets. However, this relevant width may be very different for different polarization sets and the spectra arising from sets (2) and (4) are very much broader compared to other sets. The total range of energies covered in this figure is the same as in Fig. (4) so that absolute widths may be compared. No appreciable broadening of the kinetic-energy distribution with the increase in intensity of the second field has been found for sets (1), (3), (5), and (6). But for sets (2) and (4) the distributions are very much broadened compared to those in Fig. 4.

It is found that the dissociation through a higher-energy channel $[W'(\varepsilon')]$ becomes dominant when the half-amplitude F_2 of the second field exceeds that of the first field by an order of magnitude. For different polarization sets the branching ratios, defined as the ratio of the total dissociation through the higher-energy channel to that through the lower-energy channel, show interesting variation as function of δ_1. Figure 6 shows the branching ratio for $F_1=5\times10^{-5}$ and $F_2=10^{-3}$ at $\delta_2=0$. For this lower value of F_1, the magnitudes of branching ratio are greater for all polarization combinations. All the curves show minima at different values of δ_1, which indicates that for this combination of fields and detunings the dissociation through the lower energy channel is important only for a narrow range of values of δ_1.

ACKNOWLEDGMENTS

This work was done as part of the Indo–U.S. project sponsored by the U.S.–India Fund.

[1] X. He, O. Atabek, and A. Giusti-Suzor, Phys. Rev. A **58**, 5586 (1988).
[2] A. Giusti-Suzor, X. He, O. Atabek, and F. H. Mies, Phys. Rev. Lett. **64**, 575 (1990).
[3] R. W. Heather, Comp. Phys. Commun. **63**, 446 (1991).
[4] R. W. Heather and F. H. Mies, Phys. Rev. A **44**, 7560 (1991).
[5] F. H. Mies and A. Giusti-Suzor, Phys. Rev. A **44**, 7547 (1991).
[6] A. Giusti-Suzor and F. H. Mies, Phys. Rev. Lett. **68**, 3869 (1992).
[7] H. A. Rachid, T. T. Nguyen-Dang, R. K. Chaudhuri, and X. He, J. Chem. Phys. **97**, 5497 (1992).
[8] S. Miret-Artès, O. Atabek, and A. D. Bandrauk, Phys. Rev. A **45**, 8056 (1992).
[9] S. I. Chu, J. Chem. Phys. **94**, 7901 (1991).
[10] B. Datta and S. S. Bhattacharyya, J. Chem. Phys. **94**, 7779 (1991).
[11] B. Datta and S. S. Bhattacharyya, J. Chem. Phys. **97**, 5941 (1992).
[12] B. Datta and S. S. Bhattacharyya, J. Phys. B **26**, 921 (1993).
[13] C. Cohen-Tannoudji, J. Dupont-Roc, and G. Grynberg, *Atom-Photon Interactions: Basic Processes and Applications* (Wiley Interscience, New York, 1992), Chap. 3.
[14] B. W. Shore, *The Theory of Coherent Atomic Excitation* (Wiley, New York, 1990), Chap. 20, p. 1367.
[15] B. Girard, G. O. Sitz, R. N. Zare, N. Billy, and J. Vigue, J. Chem. Phys. **97**, 26 (1992).
[16] R. G. Bray and M. Hochstrasser, Mol. Phys. **31**, 412 (1976).
[17] K. Chen and E. Yeung, J. Chem. Phys. **69**, 43 (1978).
[18] K. Chen and E. Yeung, J. Chem. Phys. **72**, 4723 (1980).
[19] S. Banerjee, M. K. Chakrabarti, S. S. Bhattacharyya, and S. Saha, J. Chem. Phys. **96**, 4974 (1992).
[20] S. Banerjee, M. K. Chakrabarti, S. S. Bhattacharyya, and

S. Saha, J. Chem. Phys. **95**, 1608 (1991).
[21] R. N. Zare, *Angular Momentum* (Wiley, New York, 1988).
[22] K. Rzazewski and J. H. Eberly, Phys. Rev. A **27**, 2026 (1983).
[23] W. Leonski and R. Tanas, J. Phys. B **21**, 2835 (1988); J. Opt. Soc. Am. B **8**, 6 (1991).
[24] C. Rongquing, X. Zhizan, S. Lan, Y. Guanhua, and Z. Wenqui, Phys. Rev. A **44**, 558 (1991).
[25] A. Carrington and R. A. Kennedy, Mol. Phys. **56**, 935 (1985); R. E. Moss and I. A. Sadler, *ibid.* **61**, 905 (1987).